MECHANICAL AND OPTICAL PROPERTIES OF NANOSTRUCTURED THIN FILMS FABRICATED BY OBLIQUE ANGLE DEPOSITION

by

Jing Wang

A Thesis Submitted to the Graduate

Faculty of Rensselaer Polytechnic Institute

in Partial Fulfillment of the

Requirements for the degree of

MASTER OF SCIENCE

Major Subject: MECHANICAL ENGINEERING

Approved:

_____

E. Fred Schubert, Thesis Advisor

_____

Michael K. Jensen, Thesis Advisor

Rensselaer Polytechnic Institute
Troy, New York

August, 2011

CONTENTS

LIST OF TABLES

LIST OF FIGURES

ACKNOWLEDGMENT

Two years' graduate study is passing so fast. I had great time during these two years at RPI. It is a great pleasure to thank those who made this thesis possible.

First and foremost, I would like to express my sincere gratitude to my advisor Professor Schubert. He gave me directions and instructions for my research. He helped and offered invaluable assistance, support and guidance. I also would like to thank him for providing me a perfect environment for my research work.

I would like to thank my co-advisor Professor Jensen. Thank for his suggestions, guidance, and helpful advice to my research. I also would like to thank my committee member Professor Picu. Thank for his advices to my qualifying exam. I got lots of help from him for my research and course work.

Successful completion of my master thesis is not possible without the help from my labmates and collaborators. I'm very happy to have this opportunity and to meet so many wonderful people during my graduate study in RPI.

I would like to thank Dr. Jingqun Xi. Without his help and encouragement, I couldn't have the opportunity to do this meaningful work. Whenever I met a problem, his advice led me to the right way. Also Dr. Xi's research attitude and hard working affect me a lot.

I would like to thank Dr. Frank Mont, An Mao, and Ardavan Zandiatashbar. Discussion with them helped me think thoroughly for the research. Thanks to them for assisting me during the preparation and completion of this thesis. Without their corporation I could not have obtained valuable data.

I would like to convey thanks to former graduate students in our group: Dr. Martin Schubert, Dr. Roya Mirhosseini, Dr. Sameer Chhajed, Dr. Jiuru Xu, Dr. Wonseok Lee,

Dr. Di Zhu, and Dr. Qi Dai. Thank them for helping me, giving me training and advice for my research. I also learned a lot from them.

I would like to thank Dr. Jaehee Cho and the current graduate students in our group. Dr Cho's patience and guidance to my research helped me a lot to go through two-year study. I thank the current group members for sharing valuable insights in my study and experiment. My special thanks to David Meyaard and Guan-Bo Lin for their support and help to my thesis work.

I would like to thank Ms. Gina Moore and Mr. John Schatz for expert administrative and technical assistance.

Finally, but most importantly, I would like to show my appreciation to my beloved family: my dearest parents, brother and husband. I thank them for their understanding and endless love through the duration of my studies. I could feel their support and love every day. I would like to express my special love and gratitude to my soul mate, my husband, Yanliang Zhang. There is no word that I could use to convey my appreciation to him. He is always supportive to my research work and my life. His love, his smile, his encouragement and his tolerance make me feel surrounded by love every day. Without my husband's encouragement, I couldn't finish my study and thesis.

ABSTRACT

The history and employment of thin films are reviewed in the first part of this Master-of-Science thesis. After that, a major technique, oblique angle deposition (OAD), which can be used to deposit thin films, is introduced. This technique shows great potential for applications in industry.

The primary objective of this thesis is to find materials that can be used to fabricate a nanostructured thin film with elastic properties. Therefore, the mechanical properties of nanostructured thin films need to be measured.

In order to investigate the mechanical properties of nanostructured thin films which are deposited with the OAD technique, the nanoindentation method is employed to measure nanorod thin films that are composed with different materials. Finally, the refractive index and porosity of Ge thin films are studied.

Chapter 1 gives a brief introduction to thin film fabrication history and different techniques to obtain porous thin films. We show that physical vapor deposition (PVD) is a fast and efficient deposition technique that is broadly employed to fabricate thin films.

Chapter 2 discusses one important PVD techniques, the oblique angle deposition (OAD) method, which is employed to deposit all thin films consisting of nanorods in this thesis work. The relationship between thin film deposition angle α and nanorod tilt angle β, measured by a scanning electron microscopy (SEM) is illustrated and established. In the meantime, the key parameters used to do deposition are also provided in this chapter.

At the beginning of Chapter 3, the mechanical properties and measurement methods of a nanorod thin film, discussed in the literature, are introduced. Thereafter, the main method, the nanoindentation measurement, which can be employed to measure elasticity of thin films, is discussed. Next, the measurement results of nanorod thin films that are composed of Ge, ZnSe and CaF_2 materials are shown to demonstrate that Ge is a good choice to satisfy our goal. In order to further investigate the elastic property of Ge nanorods, cycles of nanoindentation of different deformation are done.

In Chapter 4, basic interference theory is introduced, which is employed as the theory of refractive index measurements. The refractive index for porous Ge thin films can be achieved by matching the experimental measurements with the theoretical model.

1. Introduction to Thin Films

A thin film is a material layer with thickness ranging from several nanometers to micrometers. The science and technology of thin films have been well developed for decades of years [1, 2]. With the rapid progress of the semiconductor industry, thin film deposition on bulk materials can be achieved by different methods [2-4]. These deposited thin films can have distinctly different properties, which normal dense materials could not achieve. This chapter will discuss the thin film deposition technology and applications.

1.1 Thin Film Deposition Technology

Basically, thin film deposition can be realized by physical vapor deposition (PVD) and chemical vapor deposition (CVD) methods. It is easy to distinguish PVD from CVD according to their deposition mechanisms.

In the PVD process, (1) the source material is vaporized by electron-beam deposition heating or by electrical resistance heating; (2) then the source material vapor is transferred to the substrate surface; (3) after that, the vapor will condense on the substrate to form certain morphology of thin films. These three basic steps are necessary for any PVD deposition process. The whole deposition process flow chart is demonstrated in Figure 1.1.

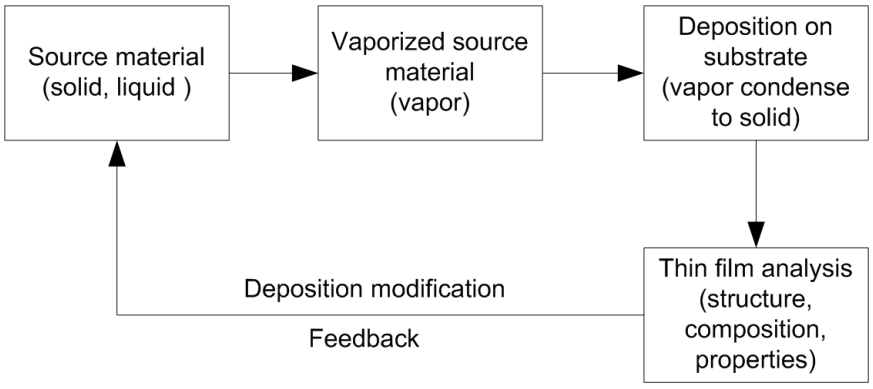

Figure 1.1 Flow chart for a thin film deposition process

PVD can be achieved by a variety of methods, including vacuum evaporation, pulsed laser deposition, sputtering deposition, and so on [5]. These PVD technologies, which are widely employed by laboratories and industries, have their own respective characteristics. Proper deposition methods need to be chosen carefully according to the requirements of the desired thin film. The comparison among two major techniques, evaporation and sputter deposition, are listed in Table 1.1.

Table 1.1 Comparison for evaporation and sputter deposition technique

Evaporation	Sputtering
High vacuum • Directional, poor step coverage • Good for lift-off	Low vacuum • Poor directionality, better step coverage • Gas atoms implanted in the film • Easier to deposit alloys
Low energy atoms (~0.1 eV)	High energy atoms/ions (1-10 eV)
Point source Poor uniformity	Parallel plate source Better uniformity
Components evaporate at different rate	All components sputtered with similar rate

In the CVD process, source materials will react with each other in the vapor phase on the substrate surface to form a thin film. According to the deposition conditions, CVD can be categorized as atmospheric-pressure CVD (APCVD), low pressure CVD (LPCVD), metal-organic CVD (MOCVD), photo-enhanced CVD (PHCVD), laser-induced CVD (LCVD), plasma-enhanced CVD (PECVD), and electron-enhanced CVD (ELCVD) [3]. These deposition methods are important ways to fabricate thin films. The materials that can be deposited by CVD are a large variety of categories.

For some materials, like metals, PVD is the first choice for thin film deposition; because it is a clean deposition process, has less processing risk, and is cost effective. For special morphologies, PVD is also preferred by researchers. However, PVD also has its own disadvantages. The uniformity, quality, and purity of thin films that are prepared by PVD are inferior to those prepared by CVD. Therefore, the deposition technique selection should be carefully considered according to the application purpose.

1.2 Thin Film Properties and Applications

With different deposition techniques, quite different thin films can be obtained. It is well known that a thin film has unique properties that a dense bulk material could not achieve, such as unique morphology, structure, and physical and chemical properties. These various characteristics enable thin films to be employed in wide areas. Table 1.2 shows the principal applications in mechanical, optical, electrical, chemical and thermal areas [2].

Table 1.2 Thin film applications [2]

Thin film property category	Typical applications
Mechanical	Tribological (water-resistant) coatings Hardness Adhesion Micromechanics
Optical	Reflective/antireflective coatings Interference filters Decoration (color, luster) Memory discs (CDs) Waveguides
Electrical	Insulation Conduction Semiconductor devices Piezoelectric driver
Chemical	Barriers to diffusion or alloying Protection against oxidation or corrosion Gas/liquid sensors
Thermal	Barrier layers Heat sinks

In the following chapters, the mechanical and optical properties and applications for porous thin films will be discussed, which is also the topic of this thesis.

Density, hardness, ductility, hardness, elasticity, adhesion, fracture and other properties are key mechanical components for thin films. The mechanical properties of thin films are quite different from those of dense bulk materials due to thin film's unique morphology, porosity, and micro structure. Thus, thin films can achieve extraordinary mechanical properties that can be practically applied.

Thin film's optical applications can be found everywhere in our daily life, which is also one of the most important application. Take lenses of optical imaging instruments as an example, such as cameras, telescopes, microscopes, optical filters, dielectric mirrors. All of them are coated with a thin film, which includes single layer coating or multi-layer coatings. In recent years, the optical applications still focus on the traditional optical equipment. However, many new optical applications have been discovered and applied for practical purpose. For instance, antireflection coatings for solar cells [6], distributed Bragg reflector (DBR) [7], end mirrors for lasers, and so on.

In summary, applications for thin films are wide. With the deposition technology development, new types of thin film characteristics can be discovered in future, which will also expand the application areas.

2. Oblique Angle Deposition

Oblique angle deposition (OAD), which is also called glancing angle deposition (GLAD), is a PVD method that can be broadly employed to deposit porous thin films [8]. In the deposition process, the substrate is covered with nanostructured materials at a high oblique angle of incidence. With this deposition technique, different columnar morphologies are formed on the substrate by changing the deposition angle and rotating the substrate [9, 10].

2.1 Oblique Angle Deposition Method

OAD, as an important PVD technique, was first proposed by D. O. Smith [11], T. G. Knorr and R. W. Hoffman [12] in 1959. They employed the self-shadowing effect discovered by H. König and G. Helwig in 1950 [13] to complete the deposition process. In the process, deposition material was heated and transformed to a vaporized particle flux which was incident on the substrate with a high oblique angle, shown as Figure 2.1. At the beginning, the particles of the source material were randomly running on the substrate, and then formed some nucleuses on the substrate. In this case, the region behind these nucleuses, which was called the shadowing region, did not receive further particle flux. As a result, a nanostructured columnar morphology could be constructed with this phenomenon. Many papers have demonstrated the property of this nanostructured columnar structure by employing the OAD technique [14].

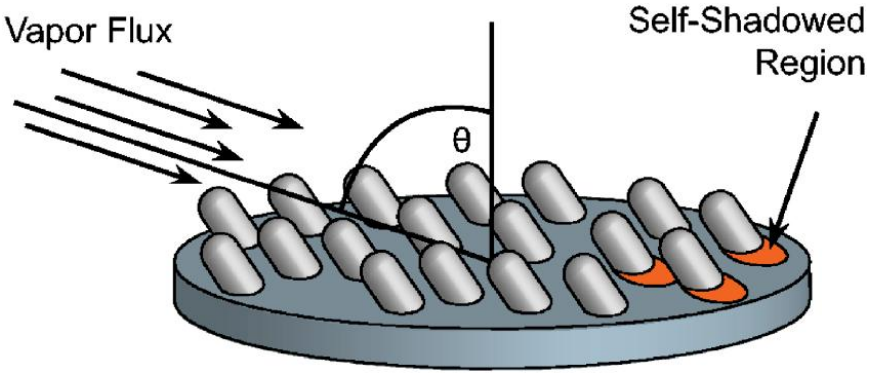

Figure 2.1 Schematic view of nanocolumn growth with self shadowing effect [7]

In 1959, N. O. Young and J. Kowal demonstrated their helically deposited fluorite films by rotating the substrate about an axis that is normal to the substrate during the deposition process [15]. In this case, the shadowing location was changed with the substrate rotation and the column growth direction was also changed in the mean time. With the substrate rotation, a spring-like nanoscale structure was formed.

OAD techniques were well explored by Robbie et al. [16, 17]. They developed the deposition system for well controlling the key process parameters, such as deposition angle, substrate rotation speed and temperature control to produce novel shapes for thin films. In summary, the incident angle of the flux and the rotation speed of substrate both determine the microstructure of the thin film [18], shown as Figure 2.2. In this figure, α is the deposition angle; φ is the substrate rotation angle around the center axis.

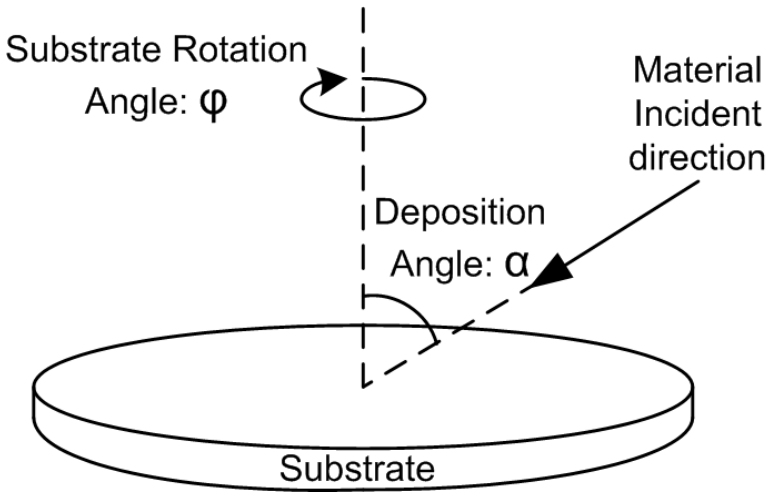

Figure 2.2 Schematic for OAD method: α is the deposition angle; φ is the substrate rotation angle.

With manipulating the incident angle and rotation speed, the microstructure will be completely different. Structures which researchers have obtained include slanted nanocolumns [19], nanotubes [20], nanoflowers [21], zigzag columns [22], spirals [23, 24], and multistack nanopillars [25]. Take two structures as examples. If the incident angle of material flux is kept constant and the substrate is maintained steady, a columnar microstructure will be formed, which can be seen clearly from scanning electron microscope (SEM) pictures. These nanostructured rods have a constant oblique angle to

the substrate, as shown in Figure 2.3 (a). If the substrate rotates 180˚ at time certain intervals during the deposition, the zigzag nanostructured columns structure will be formed, as shown in Figure 2.3 (b).

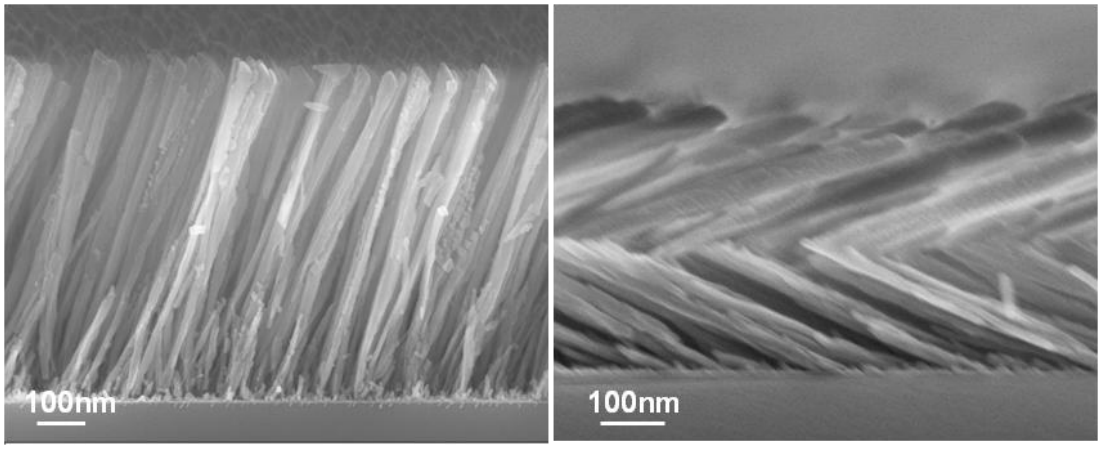

Figure 2.3 SEM pictures for (a) CaF_2 columnar nanorod (b) ZnSe zigzag nanostructured column

2.2 Electron-beam Deposition

OAD technique can be realized with different equipments, such as electron-beam deposition (EBD), iron beam deposition, sputter deposition, pulse laser deposition, and so on. In this thesis, electron-beam deposition equipment was used to fulfill the oblique angle deposition process. This process requires high vacuum environment ($< 10^{-6}$ Torr).

In the chamber of electron-beam deposition, the tungsten filament sends out an electron beam. This kind of electron-beam deposition collides with the target material and changes the material into vapor phase. The atoms of vaporized material tend to randomly roughen the substrate surface at the beginning. After that, the vaporized material will be precipitated as a solid phase on the surface to form some “seeds”, which can lead to the shadowing effect for further deposition. In other words, the region in these seed shadows does not receive the material flux, resulting in a nanostructured porous thin film. The porosity of this nanostructured thin film can be controlled by the incident angle of material flux. Nowadays, the incident angle of the material and the

rotation speed of the substrate can be controlled by computer. The larger material flux incident angle is, the more porous film will be.

In the EBD method, the deposition rate can be adjusted to low or high speed. Different materials require different deposition rate so as to get good sculpture of the nanorods. For example, the deposition rate for germanium is normally controlled within 0.6 nm/s-0.7 nm/s in this thesis. EBD method can be used for most materials. Thus it is safe and convenient to deposit different nanoscale structures. However, EBD has some disadvantages, such as being not compatible with complex geometry surfaces or inside surfaces, and the non-uniformity of the evaporation rate. When we confront this kind of difficulty, other kinds of method should be considered.

2.3 Different Angle Deposition Results for Ge

In the nanorod thin film deposition process, the tilt angle of a single nanorod (β) is different from the deposition angle (α), as shown in Figure 2.1. The relationship between these two angles has been demonstrated by many researchers [26-29].

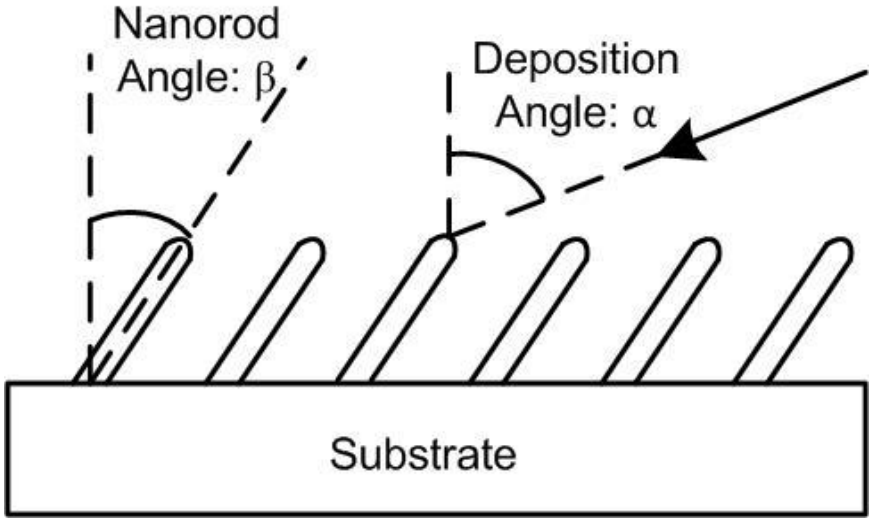

Figure 2.4 Deposition angle α and nanorod angle β

Nieuwenhuizen and Haanstra [26] proposed a tangent rule in 1966, which is described as: $\tan\alpha = 2\tan\beta$. However, this rule only can be used when deposition angle is small. In order to obtain the relationship for the deposition angle and nanorod angle when doing large angle deposition, Meakin [28] proposed another expression to describe

two angle area separately; one is for a deposition angle between 0˚ and 55˚, and the other is for angle larger than 75˚, as described below:

$$\beta = \begin{cases} C_1\alpha & for\ 0 \le \alpha \le 55^\circ \\ \alpha - C_2 & for\ \alpha \ge 75^\circ \end{cases} \quad (2\text{-}1)$$

Tait et al. [27] also derived their own expression to describe the relationship, which described as:

$$\beta = \alpha - \arcsin\left(\frac{1-\cos\alpha}{2}\right) \quad (2\text{-}2)$$

We employed electron-beam deposition to fulfill the whole nanorod thin film deposition process in this thesis work. For the purpose of exploring the relationship between deposition angle and nanorod angle, five Ge nanorod thin films were deposited on Si substrate, with same deposition height *H* but different deposition angles (reading from the quartz-crystal monitor of electron-beam system). During nanorod thin film fabrication, we set electron-beam system tooling factor as 0.74; z-value as 17.1, deposition rate as 0.6 nm/s. The deposition angles are between 65˚ and 85˚ with 5˚ interval. The thickness of thin film reading from electron-beam quartz crystal monitor is around 701 nm. With the same deposition height but different deposition angle, the heights of nanorod film measured by SEM are different, shown as Table 2.1.

Table 2.1 Ge nanorod thin film with same deposition height (on quartz-crystal monitor) but different deposition angles

Material: Ge nanorod thin film deposited on Si substrate Deposition rate: 0.6 nm/s		
Deposition angle α (degree)	Deposition height *H* reading from quartz-crystal monitor (nm)	Height *H′* measured by SEM (nm)
65	702.8	374.5
70	701.8	361.2
75	701.2	362.9
80	700.2	303.2
85	701.6	271.9

All samples' nanorod-tilt angles were measured by SEM, as shown in Table 2.1. Table 2.1 shows a certain ratio between (i) the thickness shown on the quartz-crystal

monitor and (ii) the thickness measured by SEM. This ratio allows us to control the thickness of a deposited film to meet our requirement.

The results of deposition angle α and nanorod-tilt angle β (measured by SEM) with degree and radian units for nanorod films are shown in Table 2.2. As seen from this table, the deposition angle is different from the nanorod-tilt angle that measured using SEM pictures.

Table 2.2 Oblique angle deposition with different deposition angles α and corresponding nanorod tilt angle β for Ge nanorod thin film

Material: Ge nanorod thin film deposited on Si substrate Deposition rate: 0.6 nm/s			
Deposition angle α (degree)	Deposition angle α (radian)	Nanorod-tilt angle β (degree)	Nanorod-tilt angle β (radian)
65	1.134464	46.1	0.804597
70	1.22173	47.8	0.834267
75	1.308997	52.1	0.909317
80	1.396263	58.4	1.019272
85	1.48353	60.7	1.059415

We employed Tait's formula [27] to obtain the nanorod-tilt angle β theoretically. In the mean time, we defined the relative error between theoretical angle and measured nanorod-tilt angle as：

$$Re = \frac{|\beta - \beta'|}{\beta} \tag{2-3}$$

The results are shown as Table 2.3 and drawn in Figure 2.5.

Table 2.3 Experimental and theoretical nanorod-tilt angle

Material: Ge nanorod thin film deposited on Si substrate Deposition rate: 0.6 nm/s		
Experimentally measured nanorod-tilt angle β (radian)	Theoretical nanorod-tilt angle β' (radian)	Relative error *Re* (%)

46.10	48.22	4.60%
47.80	50.79	6.26%
52.10	53.25	2.20%
58.40	55.60	4.80%
60.70	57.84	4.70%

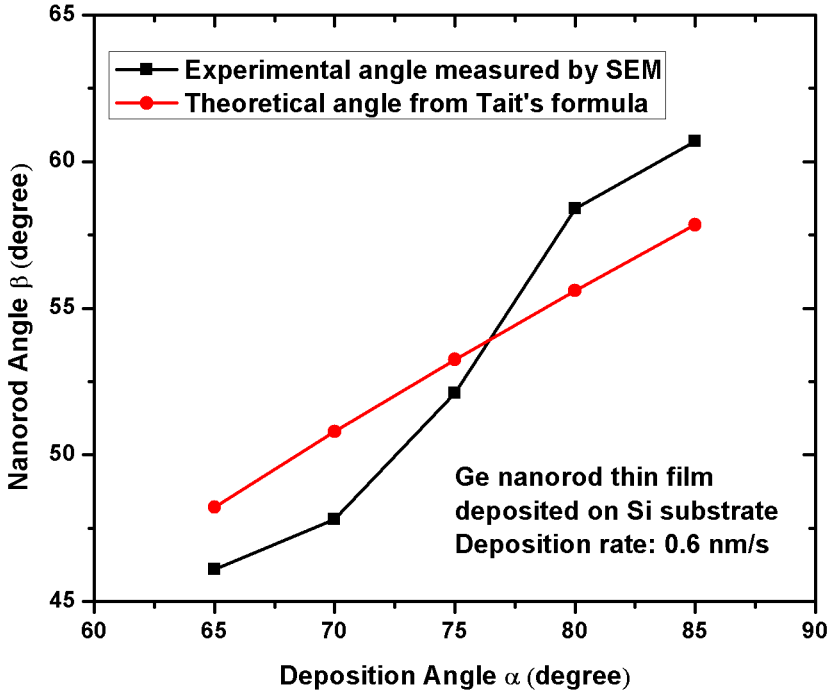

Figure 2.5 Experimental and theoretical nanorod tilt angle

In Table 2.3, the relative error between measured and calculated nanorod tilt angle illustrates that the Eq. (2-2) is a good description for their relationship. For future deposition work, Eq. (2-2) can be used to calculate the deposition angle by inserting the desired nanorod tilt angle.

2.4 Conclusion

The OAD technique and Ge OAD on Si substrate with the electron-beam deposition process were discussed and demonstrated in this chapter. During nanostructures

fabrication process, several key factors need to be considered carefully, such as pressure control of vacuum chamber, source material flow rate, deposition angle, substrate rotation rate, and deposition rate. Among these significant factors, two of them are of great importance. One is the deposition rate, which can be measured by the quartz-crystal monitor in vacuum chamber; the other one is deposition angular frequency, (i.e., the rotation speed of substrate), which can be controlled by computer. When these factors are controlled precisely, a nanostructure can be achieved with different shapes.

As one of the major methods of the PVD process, OAD is compatible with many kinds of materials, including metals, semiconductors, and dielectrics materials. The wide material compatibility is the major advantage of the OAD process. However, OAD also has its own limitation for fabricating nanostructure thin films. For example, the uniformity and precise surface morphology of OAD process is not as good as of chemical methods.

The OAD technique has been widely investigated in many areas to deposit thin films. This technique can realize specific thin film properties that conventional technique can’t achieve. Thin films which are deposited by OAD technique have interesting applications in optical, mechanic, electrical areas and many other areas.

3. Mechanical Properties of Nanostructured Thin Films

Nanostructured thin films can be constructed by employing the OAD technique, and are composed of distinctly separated columnar structures. This nanoscale structure has different mechanical properties than a continuous solid film. In recent years, the mechanical properties of OAD thin films have focused on reversibility and durability properties under external force. This thesis's purpose is to find a material whose porous thin film has good elasticity. In the mean time, this material should also be transparent in the infrared region and can be easily deposited by the PVD process.

In this chapter, we mainly investigate Ge nanostructured thin film mechanical properties by employing nanoindentation technique. Meanwhile, nanoindentation results for CaF_2 and ZnSe nanorod thin films are also included and compared with Ge thin films. Finally, we conclude that a Ge nanorod thin film has better elasticity than a film made of other materials.

3.1 Introduction to Mechanical Properties of Nanostructured Thin Films

Recently, a lot of research on mechanical properties has been done on nanostructured thin films fabricated with different materials recently. In 2005, the mechanical properties of isolated amorphous Si slanted nanorod was studied by C. Gaire et al. with Atomic Force Microscopy (AFM) [14]. They have deduced a formula to illustrate the relationship between a slanted rod's vertical deflection *d* and applied force *F* to its top end, described as Eq. (3-1). *E* is Young's modulus of the nanorod material, *I* is the axial moment of inertia of the rod cross-section, β is the nanorod-tilt angle.

$$d = \frac{FL^3 \cos^2 \beta}{3EI} \tag{3-1}$$

In 1999 and 2001, mechanical response of helical microstructured thin film was studied by M. Seto et al. by employing the nanoindentation method [30, 31]. They showed that the helical structure springs deflected elastically under low indentation force. In this paper, the authors also illustrated that a porous, microstructured SiO film is capable of being compressed more than the dense SiO films.

3.2 Introduction to the Nanoindentation Technique

In order to obtain the mechanical properties of Ge nanorod, nanoindentation measurement is a good way to achieve our goal [30-34]. There are many indentation machines from different companies that can be used to do the nanoindentation experiment. In our measurement NonoTest instrument from Micro Materials Ltd were employed. The instrument is shown as Figure 3.1. The platform is designed to support three modules: (i) nanoindentation, (ii) scanning for scratch testing, and (iii) impact [35]. In this thesis, only the nanoindentation module was employed. There are two modes for this nanoindentation equipment: load control and displacement control. Normally, for all the nanoindentation measurement in this thesis, load control mode was used. The probe that we chose to press down the thin film is a flat end diamond tip with 100 μm diameter and 60˚ slope.

Figure 3.1 The NanoTest instrument of Micro Materials Ltd [36]

During the indentation process, the sample was moved perpendicularly to the indenter. Figure 3.2 shows the schematic of relevant features of the instrument.

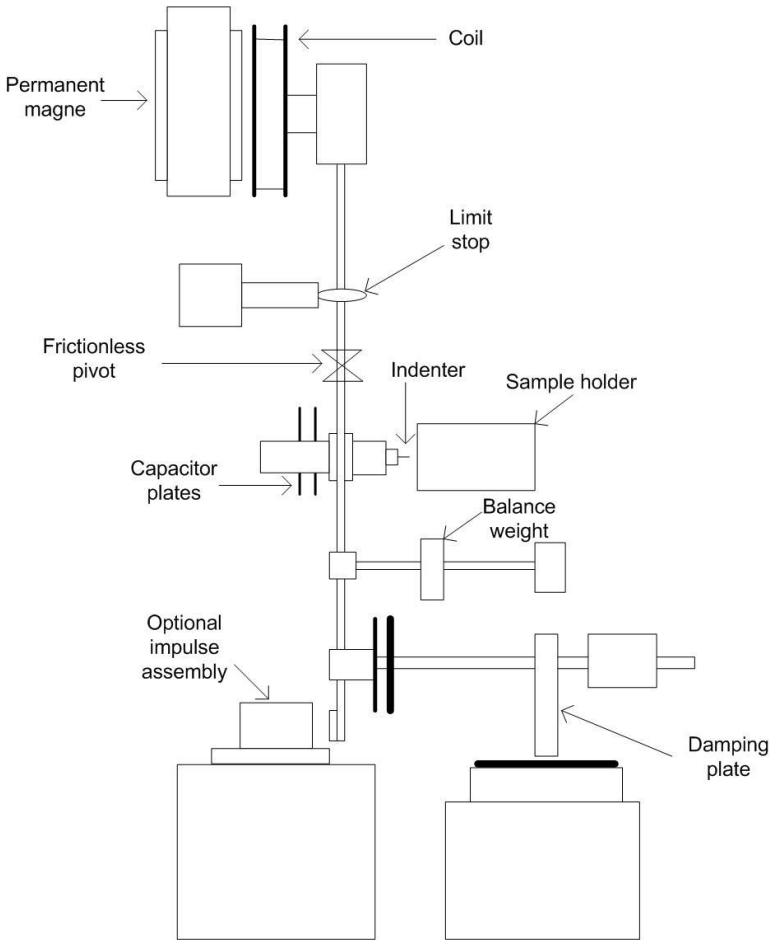

Figure 3.2 Schematic of construction for the NanoTest instrument [35]

The resulting curve of a typical nanoindentation is shown as Figure 3.3.

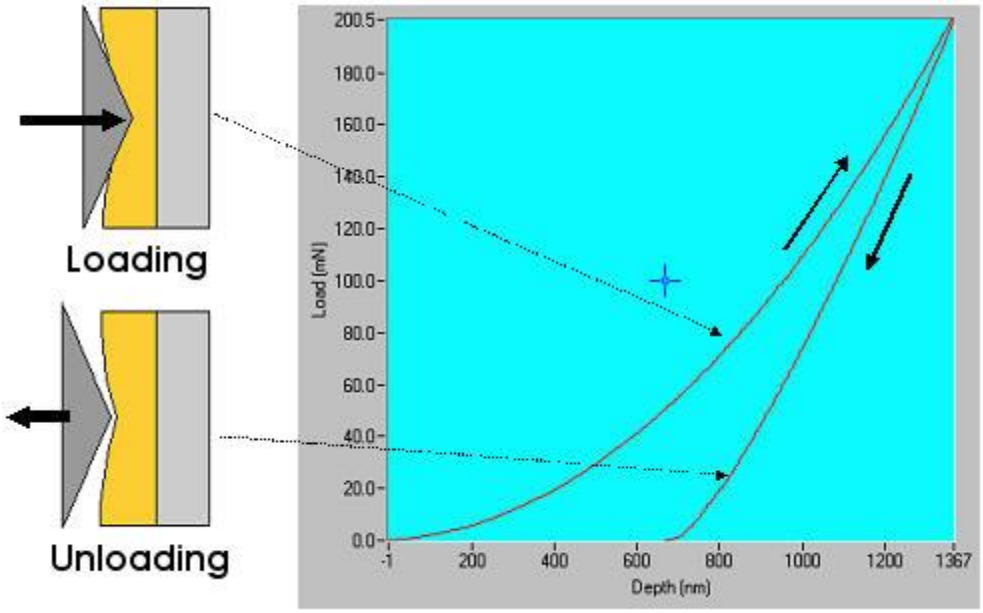

Figure 3.3 Nanoindentation result curve by using NanoTest (from Micro Materials Ltd.)

3.3 Nanoindentation Results for Ge Nanostructured Thin Film

Ge is an element of group four and an important material that can be applied in many areas. In the semiconductor field, Ge is mainly employed to make transistors, solar cells and other electronic devices. It also can be used in infrared optics systems due to its transparency property for infrared waves. Parameters of Ge are listed in Table 3.1.

Table 3.1 Parameters for Ge material

Crystal structure	Bandgap energy(eV)	Melting Point (℃)	Density (g/cm^3)	Bulk Modulus(Gpa)	Infrared refractive index n
Diamond	0.66	947	5.35	75	4

In the Ge nanostructured thin film preparation, the OAD technique was used to deposit Ge nanorods on a Si substrate by employing electron-beam deposition equipment. The Ge deposition source we utilized was 99.999% pure. The crucible that contains the Ge source material was a carbon crucible, which has little contamination

potential. The parameters' setting for the deposition is show as Table 3.2. The pressure inside the electron-beam chamber should reach less than 5×10^{-6} Torr before deposition process. The electrical current that we used was around 90 mA. The total deposition process included three cycles of operation to reach the desired thickness, because electron-beam system can not be continually operated for more than 30 minutes. Each cycle deposition thickness was around 700 nm and the deposition rate was around 0.6 nm/s.

Table 3.2 Parameters setting for Ge nanorod thin film deposition

Parameter	Value
Density	5.35 g/cm^3
Tooling factor	0.74
Z-value	17.11

During Ge nanorod thin film deposition, the deposition angle α was 85˚. The total deposition thickness reading from quartz crystal was 2.377 μm; the real thickness of this nanorod thin film reading from SEM image was 724.5 nm. The monitor deposition thickness is about 3 times larger than the real thickness of thin film by comparison.

The SEM images of top view and side view for a Ge nanorod thin film are shown as Figure 3.4. From the top view SEM image, we can tell that the Ge nanorod is not isolated very clearly. Some of the nanorod stick together to form a cluster, which can be one of the problems to affect the elasticity of Ge nanorod thin film.

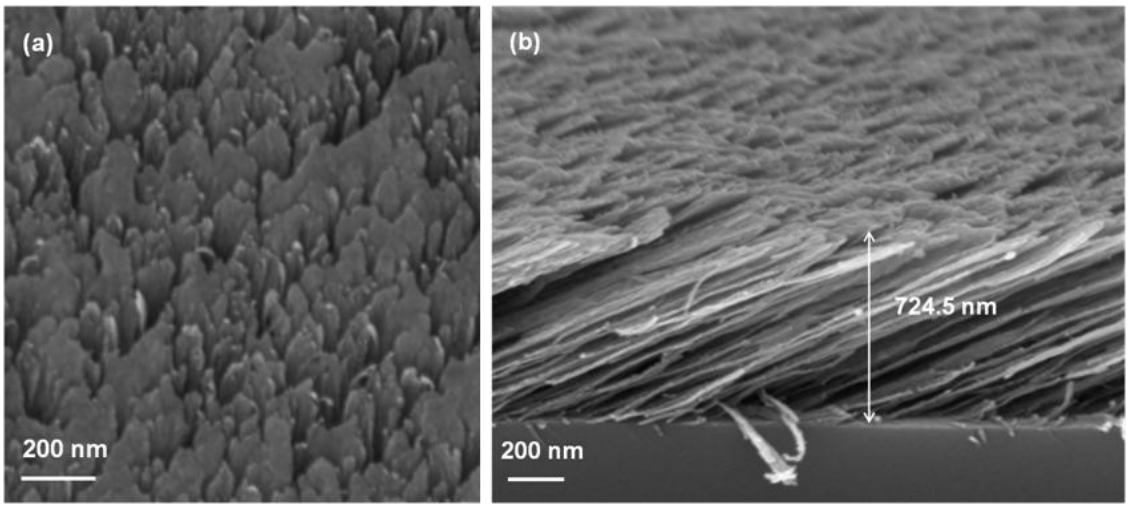

Figure 3.4 SEM images of Ge nanostructured thin film with total thickness of 724.5nm and deposition angle of 85˚, (a) top view, (b) side view

After preparation of the Ge nanorod thin film, we employed the NanoTest nanoindentation equipment to measure the mechanical properties of this thin film. During the nanoindentation measurement, the speed of the probe was 0.01 mN/s when depressing the thin film. The nanoindentation results of different indentation displacements are shown as Figure 3.5 (a) and (b).

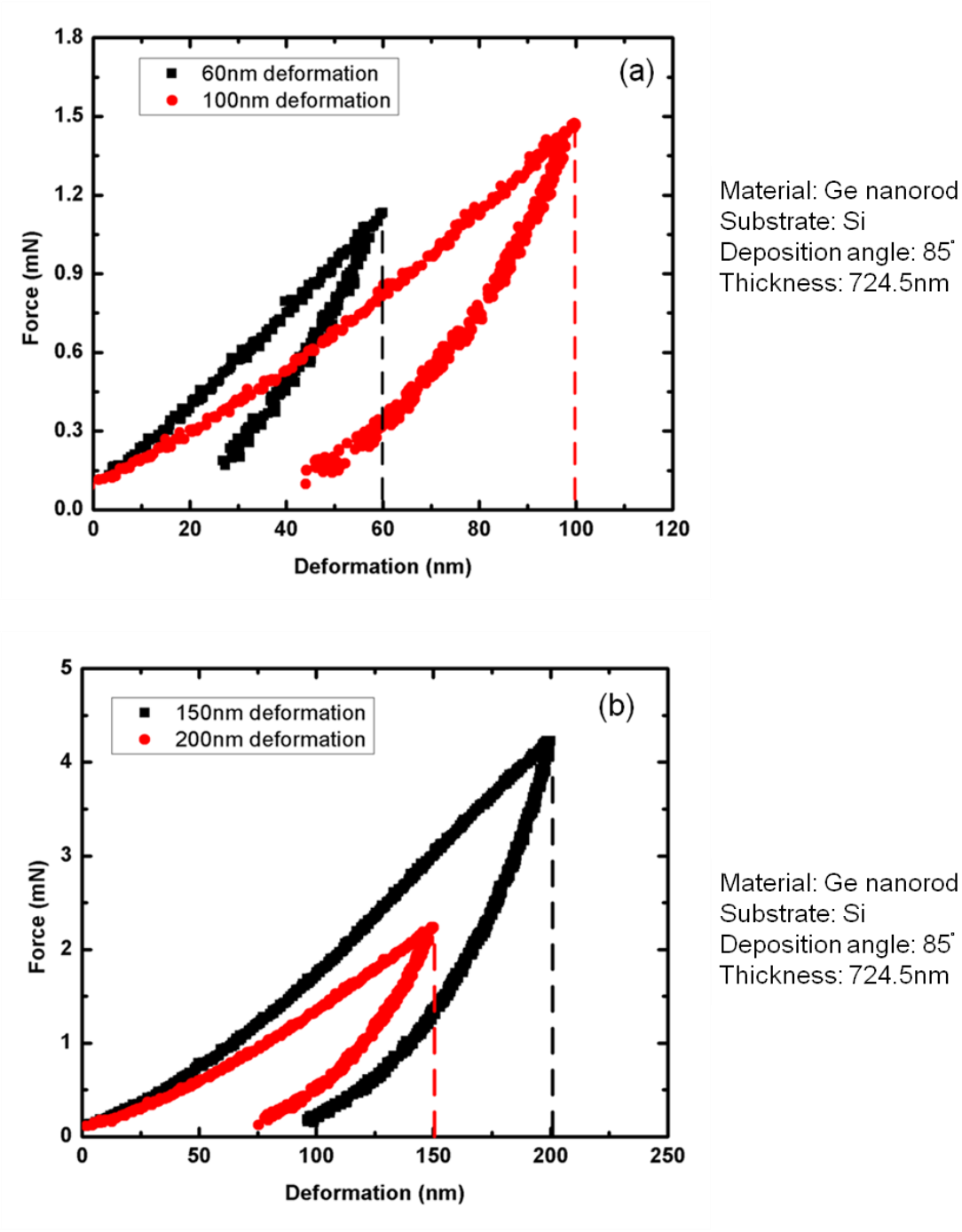

Figure 3.5 Nanoindentation results with (a) 60 nm and 100 nm deformation; (b) 150 nm and 200 nm deformation

As shown in Figure 3.5, when the film is compressed and then released, the deformation does not go to zero but goes to half of the maximum deformation. The reason for not recovering back to the original thickness can be explain as follows:

1. The nanorods might stick together during the indentation process. From the SEM photos in Figure 3.4, the distance between each pair of nanorods is not distinctly separated. Thus, there is not enough room for nanorods to bend when pressed down. The nanorods tended to touch their neighbors under compression [37].
2. The shape of Ge single nanorod doesn't fully revert after removing the load.
3. The load on thin film doesn't distribute evenly everywhere on the probe, which makes some area pressed down too much.

3.4 Nanoindentation Results for ZnSe and CaF_2 Nanostructured Thin Film

The last section discussed the nanoindentation measurement for a Ge nanostructured thin film. However, there are some other materials that can be used to deposition transparent nanostructured thin films for the infrared region. In this section, ZnSe and CaF_2 nanoindentation measurement will be introduced.

The parameters for ZnSe and CaF_2 nanorod thin films and the deposition parameters are illustrated in Table 3.3.

Table 3.3 Parameters for ZnSe and CaF_2 nanorod thin film and deposition environment

Material / Parameters	ZnSe	CaF_2
Deposition angle α ($^\circ$)	85	85
Deposition thickness t on quartz-crystal monitor (nm)	1000	1500
Nanorod thickness t' measured by SEM (nm)	261	1437
Deposition rate R (nm/s)	0.82	1.5
Deposition current I (mA)	3	25
Crucible	Carbon	Carbon
Source material purity	99.999%	99.999%

The SEM images of a ZnSe nanorod thin film with top view and side view are shown as Figure 3.6 (a) and (b) respectively, which tell the morphology information of the thin film.

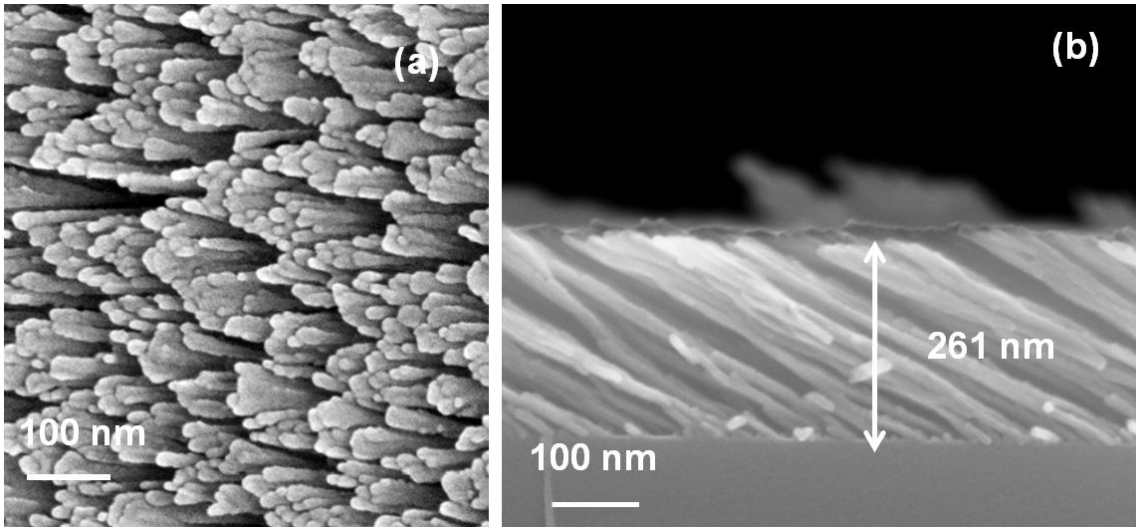

Figure 3.6 SEM images of ZnSe nanostructured thin film with total thickness of 261 nm and deposition angle of 85°, (a) top view, (b) side view

The SEM top view images of ZnSe nanorod thin film indicate that the thin film porosity was larger compared to the Ge nanorod thin film. This phenomenon is also shown in the side view: the ZnSe nanorods are separated more distinctly. However, the larger distance between ZnSe nanorods does not mean a good elastic property. The nanoindentation measurement results are shown as Figure 3.7. Comparing the same 100 nm deformation between Ge nanorod thin film and ZnSe nanorod thin film, the maximum force of Ge nanorod thin film is larger due to its smaller porosity.

Using the same nanoindentation process for Ge nanorod thin film, nanoindentation measurements are performed on ZnSe nanorod thin film to gain its mechanical property. The result of depressing force verses deformation is shown in Figure 3.7.

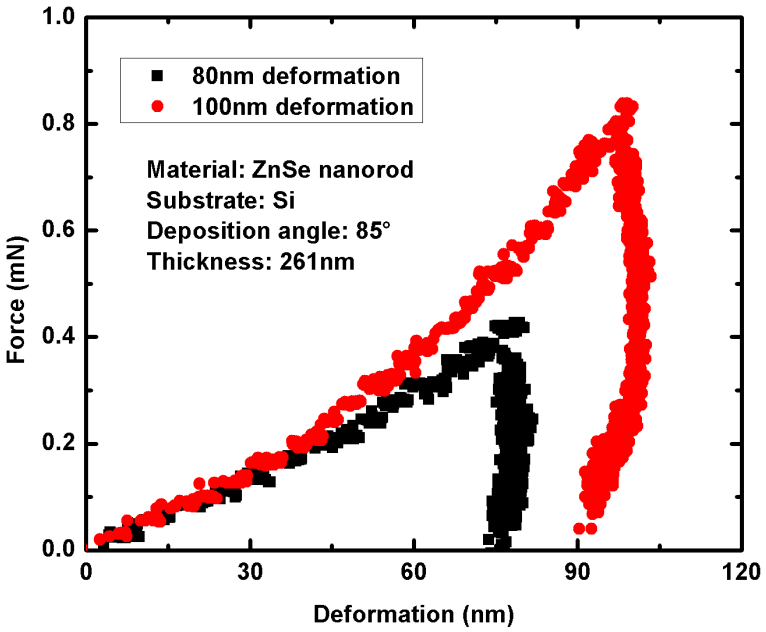

Figure 3.7 Nanoindentation results with 80 nm and 100 nm deformation for ZnSe nanorod thin film

In the 80 nm deformation unloading process, the curve stays at 80 nm according to the results of Figure 3.7. It means the ZnSe nanorod thin film did not revert at all after the loading is removed. In the 100 nm deformation unloading process, the curve goes back to 90 nm when the loading removed. This indicates that the deformation only recovers 10 nm.

In summary, the elastic property of ZnSe nanorod thin film is not as good as Ge nanorod thin film. ZnSe is not a good choice to fabricate nanorod thin film with good elasticity.

Another material that we use in this thesis was CaF_2, which is also transparent in the infrared region. The SEM images of a CaF_2 nanorod thin film with top view and side view are shown as Figure 3.8 (a) and (b).

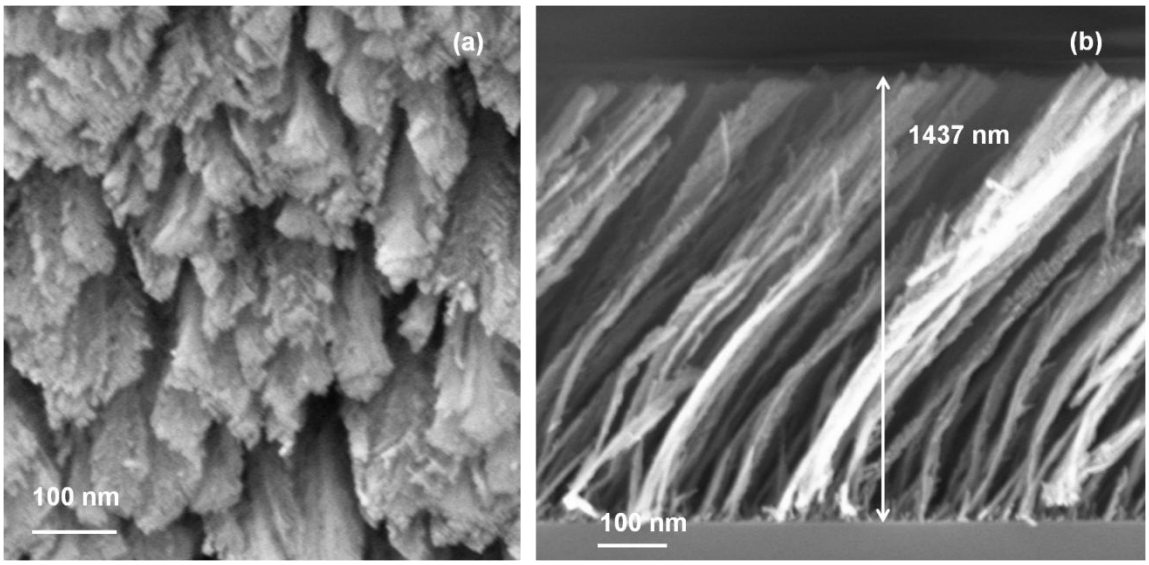

Figure 3.8 SEM images of CaF_2 nanostructured thin film with total thickness of 261 nm and deposition angle of 85°, (a) top view, (b) side view

As shown in SEM images of the CaF_2 nanorod thin film, the CaF_2 nanorod are separated more distinctly than the Ge nanorods. Unlike the top view of ZnSe nanorod, CaF_2 nanorod is rougher and more amorphous. In order to evaluate the elastic property of ZnSe nanorod thin film, the nanoindentation measurement has been done and the results are shown in Figure 3.7.

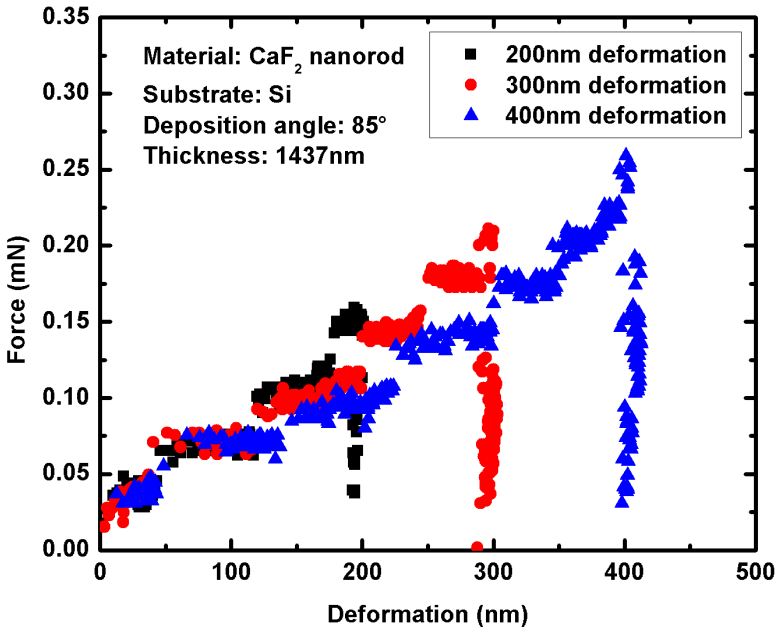

Figure 3.9 Nanoindentation results with 200 nm, 300 nm and 400 nm deformation for CaF_2 nanorod thin film

Based on the unloading process in Figure 3.9, even when the force was removed, the thin film did not revert at all. This performance demonstrates a poor elastic property for the CaF_2 nanorod thin film. The reason for this poor elastic property probably is because all the nanorods under probe were pressed down during the loading process and each single nanorod had been deformed completely. As shown in Figure 3.9, the deformation remains constant after the load has been removed. This is the typical characteristic of plastic deformation.

Considering the elastic performance of Ge, ZnSe, and CaF_2 nanorod thin films, Ge is a good material choice for depositing tunable thin films with good elasticity to satisfy our expected properties.

3.5 Nanoindentation Results for Ge Nanostructured Thin Film under Cycles of Loading and Unloading Forces

From the previous two sections, three different materials' mechanical properties were introduced. It has been proved that the Ge nanorod thin film is better than the other two

materials. However, the Ge nanorod thin film elastic property performance without cycles of loading cannot be determined from single time nanoindentation measurement. In this section, several cycles of loading and unloading processes are performed on a Ge nanorod thin film so as to get the cycled elastic information, which also can be employed to gain information on the repeatability of the nanoindentation measurement.

For the sample preparation, an electron-beam system was used to deposit total thickness of 460 nm Ge nanorod thin films with deposition rate 0.6 nm/s.

In the experiment, 5 cycles of nanoindentation were performed on Ge nanorod thin film with a maximum 300 nm displacement. The displacement and force varied with time, as shown in Figure 3.10. The probe's indentation rate was 0.01 mN/s. As seen from Figure 3.10, the minimum unloading force reaches 20% percent of the maximum loading force instead of reaching to zero. This is because of the limitation of NanoTest nanoindentation equipment, which does not lose the touch force between probe and the thin film.

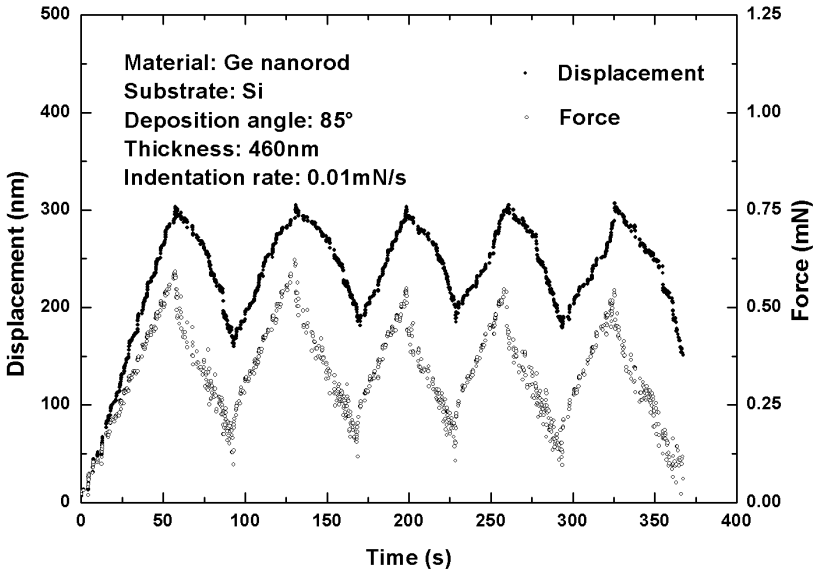

Figure 3.10 Displacement and force change with time for 5 cycles of nanoindentation measurement in displacement control mode (maximum displacement is 300 nm)

The result of 5 cycles of nanoindentation measurement is demonstrated in Figure 3.11. The data of measurement result are distributed in a certain loading and unloading loop, which almost overlapped with each other. The reason for forming loops can be explained as the friction between probe and nanorod thin film. In other words, the friction directions between two surfaces are opposite when getting load and removing load. The Figure 3.11 proves that the Ge nanorod thin film performs not well enough repeatability under the 5-cycles-nanoindentation measurement with a maximum deformation of 300 nm. This is because the 300 nm deformation is too large compared with the total thickness of 460 nm. The big deformation will change the morphology of thin film.

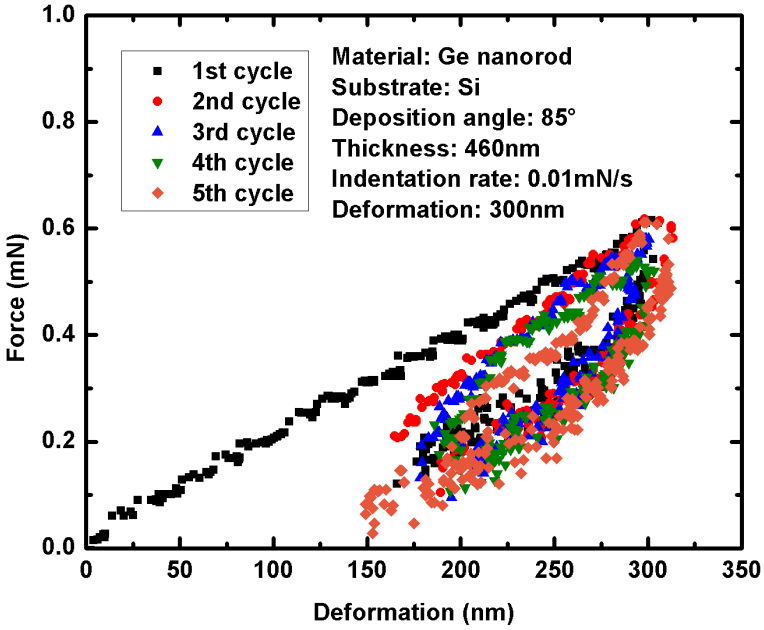

Figure 3.11 Five cycles of nanoindentation measurement for Ge nanorod thin film with maximum 300 nm deformation

Since 300 nm maximum deformation did not show a good result, a smaller deformation, 200 nm maximum deformation, was chosen to further investigate the repeatability of the measurement. With the same probe indentation rate, 10 cycles of

measurements were performed using force-control mode. Measurement results are shown in Figure 3.13. Ten cycles of loading and unloading process are overlapped with each other, which indicate excellent nanoindentation-measurement repeatability of Ge nanorod thin film. However, the elastic property of the thin film with ten cycles' compression behaves not as well as one cycle compression. From the previous section, the nanorod thin film reverted back to half of the maximum deformation. From Figure 3.12, the thin film only recovers back to 140 nm with 200 nm maximum deformation, which means the good measurement repeatability sacrifices good elasticity under 10 cycles compression.

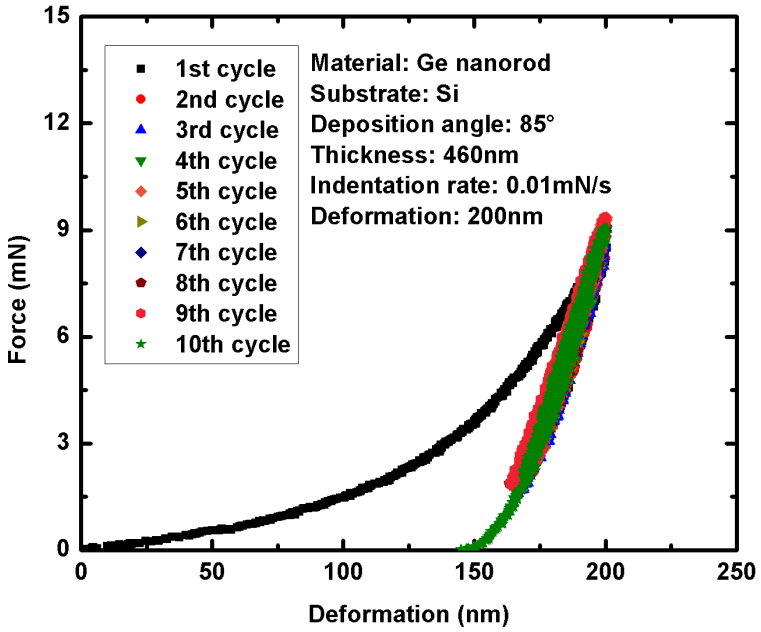

Figure 3.12 Ten cycles of nanoindentation measurement for Ge nanorod thin film with maximum 200 nm deformation

With the same probe indentation rate 0.01 mN/s, 5 cycles of measurement were performed in the force-control mode, as shown in Figure 3.13. The maximum force limitation in this experiment is 0.5 mN. As can be seen in Figure 3.13, the displacement reached a maximum value at the peak displacement.

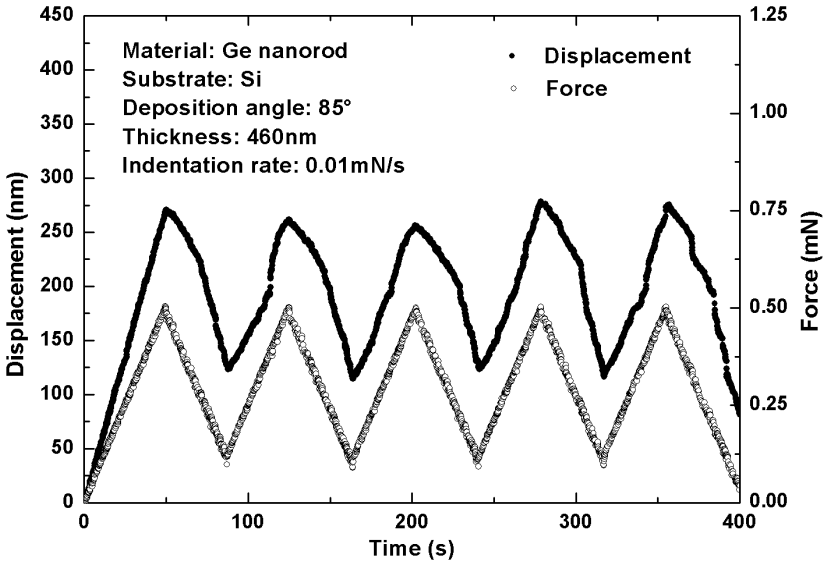

Figure 3.13 Displacement and force change with time for 5 cycles of nanoindentation measurement in force control mode (maximum force is 0.50 mN)

The five cycles nanoindentation results for a Ge nanorod thin film are shown in Figure 3.14. The result curve of 5 cycles' nanoindentation measurements are overlapped and repeated, which proves good measurement repeatability of Ge nanorod thin film. As seen from Figure 3.14, the curve goes back to 50 nm after the fifth cycle unloading process, which means a good elastic property for Ge nanorod thin film. In this measurement, the total deformation that was pressed down is 300 nm. The deformation went back to 50 nm after removing the force, which indicates that 250 nm-displacement reverted. This shows the excellent elastic property of Ge nanorod thin film.

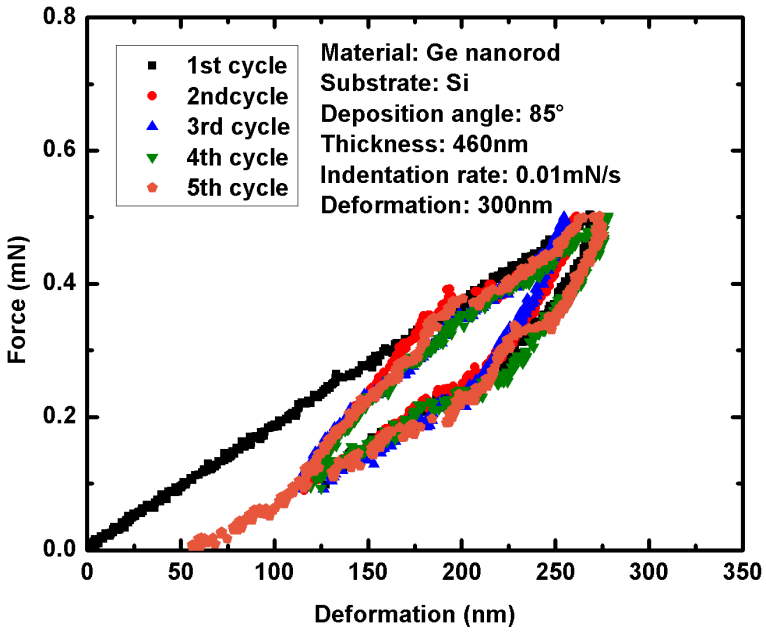

Figure 3.14 Five cycles of nanoindentation measurement for Ge nanorod thin film with maximum 0.5 mN compressive force

From previous measurement results, the Ge nanorod thin film has been proved to be a good elastic material that can be employed to reach our goal. And the nanoindentation-measurement repeatability of the Ge nanorod thin film shows repeatable and credible.

3.6 Conclusion

In this chapter, the literature on mechanical properties of thin films was reviewed. The measurement method that can be used to test thin film's mechanical property was introduced. The nanoindentation-measurement results of Ge, ZnSe and CaF_2 nanorod thin film were used to determine which material was better suited to fulfill the requirements. In order to further test the elastic performance of Ge nanorod thin film, several cycles of nanoindentation measurement were performed.

Thin films which are composed of distinctly separated nanorods have advantageous properties compared with the same material in dense bulk films. In this chapter, the mechanical property of nanorod thin film has been investigated by a nanoindentation instrument. It has been proved that a Ge nanorod thin film has a good elasticity property

under repeated loading and unloading forces. The unusual mechanical characteristic of nanorod thin film can be widely applied in many interesting areas.

S. V. Kesapragada and his co-workers [37] deposited Cr zigzag nanosprings on SiO_2/Si substrates. They found that the array of Cr nanosprings exhibit reversibility under loading and unloading, which indicates their potential as pressure sensors [37]. In that paper, they also demonstrated that loads larger than 1MPa caused irreversible plastic deformation and degraded the pressure sensitivity.

J. P. Singh et al. [38] also demonstrated a nanoscale electromechanical actuator operation by employing mechanical properties of isolated nanostructured springs. In their work, a thin film was deposited with four-turn Si nanosprings by using OAD technique, and then deposited 10 nm thick Co layer coating on the top of the Si nanosprings by using the CVD process. This nanospring thin film was compressed by passing through a DC current with AFM tip. They verified it was possible to electromechanically actuate nanospring structured thin films within a 6 nm displacement. With their demonstration, the electromechanical actuator could be realized and integrated into micro systems.

4. Simulation of Optical Properties of Ge Nanostructured Thin Film

OAD technique is a well-known deposition method that has been employed to fabricate optical coatings. The optical properties for nanostructured thin films deposited with the OAD method are one of the important properties. Such films can be widely applied in many areas, such as photonic crystals [17, 24, 39], antireflection coating [40-44], mirrors, and optical filters [45-49] and so on. In this chapter, the theory of optical interference for thin films is firstly introduced. Then the optical property simulation results on Ge nanostructured thin film are discussed.

4.1 Introduction to Optical Properties of Thin Films

As early as 1953, some investigations had been done on the optical anisotropy to obliquely deposited films [50]. After that, transparent materials deposited by OAD technique with metal oxide were discovered to have birefringent properties [51]. Another important research about thin films deposited by OAD method is the antireflection coating, which has been broadly investigated for many years [7, 52-55]. In the research work of Tait et al. [27], an expression that relates thin film density ρ and the deposition angle α is illustrated as Eq. (4-1).

$$\rho = \frac{2\,cos\alpha}{1 + cos\alpha} \tag{4-1}$$

Eq. (4-1) shows the density changes with the deposition angle, and it indicates the porosity of thin film can be manipulated by changing the deposition angle. In the meantime, the refractive index will also be changed automatically. In order to obtain antireflection coating, a graded index layer should be employed to make a smooth transition from the top layer index to the substrate index [44].

For obliquely deposited thin films, interference is an important optical phenomenon which occurs when two light waves interfere with each other to form a new light wave. One of the light waves is reflected by the top surface of the thin film; the other light wave is refracted into the thin film and reflected by the bottom surface, as shown in Figure 4.1.

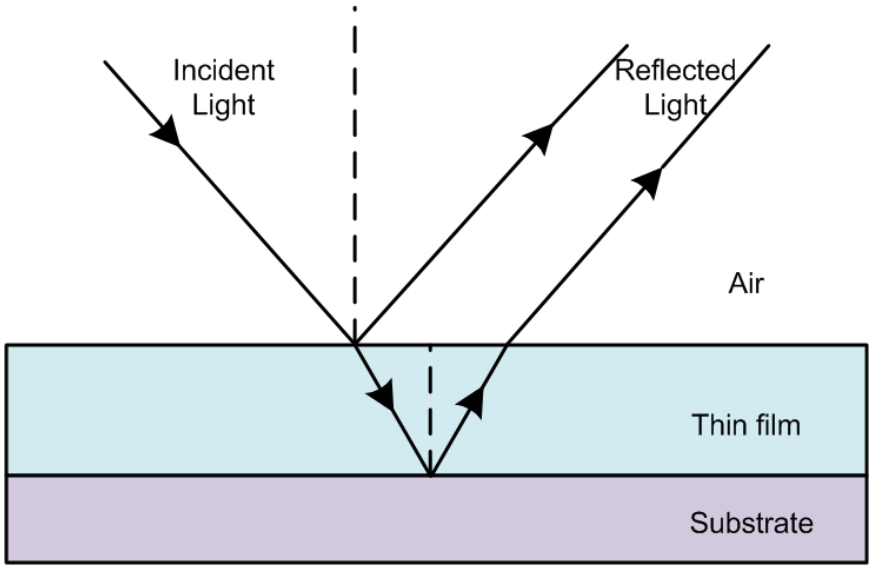

Figure 4.1 Interference of incoming light wave by a thin film top and bottom surface

As indicated in Figure 4.1, the two reflected light waves will interfere with each other to form an interference pattern. This phenomenon could be seen almost every day, such as the soap bubbles, oil floating on water, laser disk surface, and so on. The interference pattern of thin film depends on the thickness and refractive index of itself. In this work, we keep the thin film thickness the same, but change the refractive index by altering thin film's deposition angle to see how the refractive index change.

4.2 Reflectivity Change of Ge Nanorod Thin Film Deposited at Different Deposition Angles

Thin film that fabricated under oblique angle is porous. Its porosity depends on the deposition angle. It has been shown that the porosity is getting larger with deposition angle increase. In order to get high porosity thin film, the deposition angle is normally larger than 80˚.

There is a linear formula which describes the relationship between the dense material's refractive index n_{dense}, thin film refractive index n_{film}, and the porosity p, shown as Eq. (4-2).

$$n_{film} = n_{dense} \times (1 - p) + 1 \times p \tag{4-2}$$

The porosity of thin film is defined as the ratio between the volume of air in the film to the total volume of the film [56], which includes the volume of air and dense material, as described in Eq. (4-3). V_{air}, V_{total}, V_{dense} are the volume of air, total thin film, and dense material respectively.

$$p = \frac{V_{air}}{V_{total}} = \frac{V_{air}}{V_{air} + V_{dense}} \tag{4-3}$$

In experiments, the reflectivity can be measured by a spectrophotometer. Take a Ge nanorod thin film as an example, which is deposited to 271.9 nm thickness with 85° deposition angle on a Si substrate. The refractive index of this porous Ge thin film will be lower than a dense Ge thin film. In order to determine the new refractive index, the refractive index in a simulation should be changed to fit the measurement curve of reflectance. The fitting requires that the peak and valley points of both curves occur at the same wavelength. The measured and calculated results are show in Figure 4.2. According to fitting result, the refractive index *n* of this nanorod thin film is 1.8, and the porosity *p* is 73.3% calculated from Eq. (4-2).

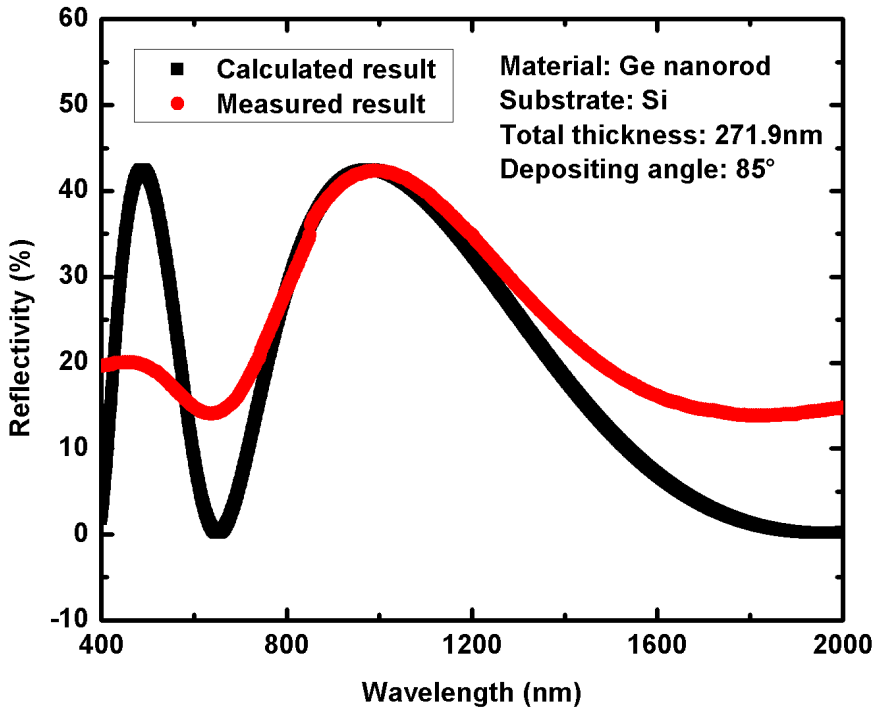

Figure 4.2 Calculated and measured results of 260 nm Ge nanorod thin film

As seen from Figure 4.2, the peak and valley points of the calculated curve have the same wavelengths as the measured curve, which means that the fitting curve fulfills the requirement. The refractive index and the porosity could be applied to any thickness Ge thin film that is deposited at 85˚ on a Si substrate.

With the same fitting method, the porosities of thin films under different deposition angle are listed as below:

Table 4.1 Porosities of thin films under different deposition angle

Deposition Angle (˚)	Porosity (%) calculated from Eq. (4-2)	Refractive Index n_{film} calculated from Eq. **Error! Reference ource not found.**)
70	10.3%	3.69
75	24.0%	3.28
80	52.0%	2.44
85	73.3%	1.80
88	76.3%	1.71

As shown in Table 4.1, with the thin film deposition angle incensement, its refractive index will decrease and the porosity will increase.

4.3 Robust nanorod optical thin films

Nanorod thin films with low refractive index values are a new class of optical thin films. They provide a variety of refractive index values that conventional optical thin films cannot achieve. Therefore, they have great potential for use in optical coating applications. Optical coatings are widely used in industry to achieve a specific optical performance. However, the robustness of the optical coatings themselves is required due to the fact that optical coatings usually also serve as protective layers on the surface. Nanorod thin films have lower hardness and durability due to the increased porosity compared to dense thin films. As a result, mechanical pressing or surface scratching can easily damage the thin films and hence the optical performance of the optical coatings.

Therefore, the mechanical robustness of the nanorod thin films is a major reason that has limited their adoption by the optical thin film community.

Our mechanical measurement shows that some nanorod thin films, such as Ge nanorods, have good elasticity. This can provide the possibility to achieve nanorod optical thin films for maintaining the optical performance integrity while under mechanical stress forces such as pressing. Elasticity of the nanorod thin film allows it to recover to its original status after the mechanical pressing. As a result, the optical characteristics of the nanorod thin films can be recovered too. Therefore, a robust nanorod optical thin film can be achieved by choosing a nanorod thin film with good elasticity.

4.4 Conclusion and Future Work

The optical properties of Ge nanorod thin film have been analyzed for both experiments and simulations in this chapter. It has been demonstrated that the refractive index and porosity of Ge nanorod thin film can be manipulated by depositing Ge at different vapor flux incident angles.

The optical properties of Ge nanorod thin film have been simulated by employing optical interference equations in this chapter. There will be a great potential to explore other material's optical properties with single and multi-layers for future work.

5. References

1. M. Ohring, The materials science of thin films (Academic Press, 1992).

2. D. L. Smith, Thin-film deposition: principles and practice (McGraw-Hill Professional, 1995).

3. K. Seshan, Handbook of thin-film deposition processes and techniques: principles, methods, equipment and applications (William Andrew, 2002).

4. R. Glang, and L. I. Maissel, Handbook of thin film technology (McGraw-Hill, 1970).

5. D. M. Mattox, and ScienceDirect, Handbook of physical vapor deposition (PVD) processing (William Andrew, 2010).

6. A. Prasad, S. Balakrishnan, S. Jain, and G. Jain, "Porous Silicon Oxide Anti Reflection Coating for Solar Cells," Journal of the Electrochemical Society 129, 596 (1982).

7. M. F. Schubert, J. Q. Xi, J. K. Kim, and E. F. Schubert, "Distributed Bragg reflector consisting of high-and low-refractive-index thin film layers made of the same material," Applied Physics Letters 90, 141115 (2007).

8. M. J. Brett, and M. M. Hawkeye, "MATERIALS SCIENCE: New Materials at a Glance," Science 319, 1192 (2008).

9. K. Robbie, L. Friedrich, S. Dew, T. Smy, and M. Brett, "Fabrication of thin films with highly porous microstructures," Journal of Vacuum Science & Technology A: Vacuum, Surfaces, and Films 13, 1032-1035 (1995).

10. K. Robbie, and M. Brett, "Sculptured thin films and glancing angle deposition: Growth mechanics and applications," Journal of Vacuum Science & Technology A: Vacuum, Surfaces, and Films 15, 1460-1465 (1997).

11. D. O. Smith, "Anisotropy in permalloy films," Journal of Applied Physics 30, S264-S265 (1959).

12. T. Knorr, and R. Hoffman, "Dependence of geometric magnetic anisotropy in thin iron films," Physical Review 113, 1039-1046 (1959).

13. H. Konig, and G. Helwig, "The Structure of Obliquely Evaporated Films and Their Influence on the Formation of Sub-Microscopic Surface Irregularities," Optik 6, 111 (1950).

14. C. Gaire, D. Ye, F. Tang, R. Picu, G. Wang, and T. Lu, "Mechanical testing of isolated amorphous silicon slanted nanorods," Journal of Nanoscience and Nanotechnology 5, 1893-1897 (2005).

15. N. O. Young, and J. Kowal, "Optically active fluorite films," Nature 183, 104-105 (1959).

16. K. Robbie, M. Brett, and A. Lakhtakia, "Chiral sculptured thin films," Nature 384 (1996).

17. K. Robbie, D. Broer, and M. Brett, "Chiral nematic order in liquid crystals imposed by an engineered inorganic nanostructure," Nature 399, 764-766 (1999).

18. M. M. Hawkeye, and M. J. Brett, "Glancing angle deposition: Fabrication, properties, and applications of micro-and nanostructured thin films," Journal of Vacuum Science & Technology A: Vacuum, Surfaces, and Films 25, 1317 (2007).

19. D. Ye, T. Karabacak, R. Picu, G. Wang, and T. Lu, "Uniform Si nanostructures grown by oblique angle deposition with substrate swing rotation," Nanotechnology 16, 1717 (2005).

20. S. Kesapragada, P. Sotherland, and D. Gall, "Ta nanotubes grown by glancing angle deposition," Journal of Vacuum Science & Technology B: Microelectronics and Nanometer Structures 26, 678 (2008).

21. Y. P. Zhao, D. X. Ye, G. C. Wang, and T. M. Lu, "Novel nano-column and nano-flower arrays by glancing angle deposition," Nano Letters 2, 351-354 (2002).

22. R. Messier, V. C. Venugopal, and P. D. Sunal, "Origin and evolution of sculptured thin films," Journal of Vacuum Science & Technology A: Vacuum, Surfaces, and Films 18, 1538 (2000).

23. Y. Zhao, D. Ye, P. I. Wang, G. Wang, and T. Lu, "Fabrication of Si nanocolumns and Si square spirals on self-assembled monolayer colloid substrates," International Journal of Nanoscience 1, 87-97 (2002).

24. S. R. Kennedy, M. J. Brett, O. Toader, and S. John, "Fabrication of tetragonal square spiral photonic crystals," Nano Letters 2, 59-62 (2002).

25. S. Kesapragada, and D. Gall, "Two-component nanopillar arrays grown by Glancing Angle Deposition," Thin Solid Films 494, 234-239 (2006).

26. J. Nieuwenhuizen, and H. Haanstra, "Microfractography of thin films," Philips Technical Review 27, 87-91 (1966).

27. R. Tait, T. Smy, and M. Brett, "Modelling and characterization of columnar growth in evaporated films," Thin Solid Films 226, 196-201 (1993).

28. P. Meakin, "Ballistic deposition onto inclined surfaces," Physical Review A 38, 994-1004 (1988).

29. S. Lichter, and J. Chen, "Model for columnar microstructure of thin solid films," Physical Review Letters 56, 1396-1399 (1986).

30. M. Seto, K. Robbie, D. Vick, M. Brett, and L. Kuhn, "Mechanical response of thin films with helical microstructures," Journal of Vacuum Science & Technology B: Microelectronics and Nanometer Structures 17, 2172 (1999).

31. M. W. Seto, B. Dick, and M. J. Brett, "Microsprings and microcantilevers: studies of mechanical response," Journal of Micromechanics and Microengineering 11, 582 (2001).

32. T. F. Page, and S. V. Hainsworth, "Using nanoindentation techniques for the characterization of coated systems: a critique," Surface and Coatings Technology 61, 201-208 (1993).

33. G. Pharr, and W. Oliver, "Measurement of thin-film mechanical-properties using nanoindentation," Mrs Bulletin 17, 28-33 (1992).

34. G. Pharr, and A. Bolshakov, "Understanding nanoindentation unloading curves," Journal of Materials Research 17, 2660-2671 (2002).

35. A. C. Fischer-Cripps, Nanoindentation (Springer Verlag, 2004).

36. M. M. Ltd, "http://www.micromaterials.co.uk/." Date Last Accessed, 06/20/2011.

37. S. Kesapragada, P. Victor, O. Nalamasu, and D. Gall, "Nanospring pressure sensors grown by glancing angle deposition," Nano Letters 6, 854-857 (2006).

38. J. Singh, D. L. Liu, D. X. Ye, R. Picu, T. M. Lu, and G. C. Wang, "Metal-coated Si springs: Nanoelectromechanical actuators," Applied Physics Letters 84, 3657 (2004).

39. S. L. Kuai, X. F. Hu, A. Hache, and V. V. Truong, "High-quality colloidal photonic crystals obtained by optimizing growth parameters in a vertical deposition technique," Journal of Crystal Growth 267, 317-324 (2004).

40. M. L. Kuo, D. J. Poxson, Y. S. Kim, F. W. Mont, J. K. Kim, E. F. Schubert, and S. Y. Lin, "Realization of a near-perfect antireflection coating for silicon solar energy utilization," Optics Letters 33, 2527-2529 (2008).

41. D. J. Poxson, M. F. Schubert, F. W. Mont, E. Schubert, and J. K. Kim, "Broadband omnidirectional antireflection coatings optimized by genetic algorithm," Optics Letters 34, 728-730 (2009).

42. M. F. Schubert, F. W. Mont, S. Chhajed, D. J. Poxson, J. K. Kim, and E. F. Schubert, "Design of multilayer antireflection coatings made from co-sputtered and low-refractive-index materials by genetic algorithm," Applied Optics 34, 2247-2254 (2008).

43. M. F. Schubert, D. J. Poxson, F. W. Mont, J. K. Kim, and E. F. Schubert, "Performance of Antireflection Coatings Consisting of Multiple Discrete Layers and Comparison with Continuously Graded Antireflection Coatings," Applied Physics Express 3, 082502 (2010).

44. W. Southwell, "Gradient-index antireflection coatings," Optics Letters 8, 584-586 (1983).

45. H. A. Macleod, Thin-film optical filters (Taylor & Francis, 2001).

46. C. K. Madsen, and J. H. Zhao, Optical filter design and analysis (Wiley Online Library, 1999).

47. R. Magnusson, and S. Wang, "New principle for optical filters," Applied Physics Letters 61, 1022-1024 (1992).

48. D. J. Poxson, F. W. Mont, M. F. Schubert, J. K. Kim, J. Cho, and E. F. Schubert, "Demonstration of optical interference filters utilizing tunable refractive index layers," Optics Express 18, A594-A599 (2010).

49. D. Sadot, and E. Boimovich, "Tunable optical filters for dense WDM networks," Communications Magazine, IEEE 36, 50-55 (1998).

50. L. Holland, "The effect of vapor incidence on the structure of evaporated aluminum films," Journal of the Optical Society of America 43, 376–380 (1953).

51. T. Motohiro, and Y. Taga, "Thin film retardation plate by oblique deposition," Applied Optics 28, 2466-2482 (1989).

52. J. Q. Xi, J. K. Kim, and E. F. Schubert, "Silica nanorod-array films with very low refractive indices," Nano Letters 5, 1385-1387 (2005).

53. J. Q. Xi, J. K. Kim, E. Schubert, D. Ye, T. M. Lu, S. Y. Lin, and J. S. Juneja, "Very low-refractive-index optical thin films consisting of an array of SiO2 nanorods," Optics Letters 31, 601-603 (2006).

54. J. K. Kim, T. Gessmann, E. F. Schubert, J. Q. Xi, H. Luo, J. Cho, C. Sone, and Y. Park, "GaInN light-emitting diode with conductive omnidirectional reflector having a low-refractive-index indium-tin oxide layer," Applied Physics Letters 88, 013501 (2006).

55. J. Q. Xi, M. F. Schubert, J. K. Kim, E. F. Schubert, M. Chen, S. Y. Lin, W. Liu, and J. A. Smart, "Optical thin-film materials with low refractive index for broadband elimination of Fresnel reflection," Nature Photonics 1, 176-179 (2007).

56. D. Poxson, F. Mont, M. Schubert, J. Kim, and E. Schubert, "Quantification of porosity and deposition rate of nanoporous films grown by oblique-angle deposition," Applied Physics Letters 93, 101914 (2009).